

# Superconductivity induced by structural reorganization in electron-doped cuprate NCCO

Anita Guarino<sup>1,2,\*</sup>, Carmine Autieri<sup>3,2,\*</sup>, Pasquale Marra<sup>4,5,†</sup>, Antonio Leo<sup>1,2,6</sup>, Gaia Grimaldi<sup>2,1</sup>, Adolfo Avella<sup>1,2,7,‡</sup> and Angela Nigro<sup>1,2</sup>

<sup>1</sup>*Dipartimento di Fisica “E. R. Caianiello”, Università degli Studi di Salerno, 84084 Fisciano (Salerno), Italy*

<sup>2</sup>*Consiglio Nazionale delle Ricerche CNR-SPIN, UOS Salerno, 84084 Fisciano (Salerno), Italy*

<sup>3</sup>*International Research Centre Magtop, Institute of Physics,*

*Polish Academy of Sciences, Aleja Lotników 32/46, 02668 Warsaw, Poland*

<sup>4</sup>*Graduate School of Mathematical Sciences, The University of Tokyo, 3-8-1 Komaba, Meguro, Tokyo, 153-8914, Japan*

<sup>5</sup>*Department of Physics, and Research and Education Center for Natural Sciences, Keio University, 4-1-1 Hiyoshi, Yokohama, Kanagawa, 223-8521, Japan*

<sup>6</sup>*NANO\_MATES Research Center, Università degli Studi di Salerno, 84084 Fisciano (Salerno), Italy*

<sup>7</sup>*Unità CNISM di Salerno, Università degli Studi di Salerno, 84084 Fisciano (Salerno), Italy*

(Dated: December 25, 2020)

Electron-doped and hole-doped superconducting cuprates exhibit a symmetric phase diagram as a function of doping. This symmetry is however only approximate. Indeed, electron-doped cuprates become superconductors only after a specific annealing process: This annealing affects the oxygen content only by a tiny amount, but has a dramatic impact on the electronic properties of the sample. Here, we report the occurrence of superconductivity in oxygen-deficient  $\text{Nd}_{2-x}\text{Ce}_x\text{CuO}_4$  thin films grown in oxygen-free environment, after annealing in pure argon flow. As verified by x-ray diffraction, annealing induces an increase of the interlayer distance between  $\text{CuO}_2$  planes in the crystal structure. Since this distance is correlated to the concentration of oxygens in apical positions, and since oxygen content cannot substantially increase during annealing, our experiments indicate that the superconducting phase transition has to be ascribed to a migration of oxygen ions to apical positions during annealing. Moreover, as we confirm via first-principles density functional theory calculations, the changes in the structural and transport properties of the films can be theoretically described by a specific redistribution of the existing oxygens ions at apical positions with respect to  $\text{CuO}_2$  planes, which remodulates the electronic band structure and suppresses the antiferromagnetic order, allowing the emergence of hole superconductivity.

Since the discovery of superconductivity in  $\text{LaBaCuO}$  by Bednorz and Müller in 1986 [1], the family of high-temperature cuprate superconductors has grown to include more than hundreds compounds [2] with temperatures as high as 133 K at atmospheric pressure [3]. All these compounds share a similar crystal structure, made up of stacked layers of copper-oxygen planes, and fit into a universal phase diagram, where superconductivity emerges upon doping an antiferromagnetic Mott insulator [4, 5]. Indeed, when the stoichiometric parent compound is doped via ionic substitution, the antiferromagnetic phase is suppressed and superconductivity appears. Ionic substitution may result in the creation of additional holes or electrons in the  $\text{CuO}_2$  planes. Hole-doped [1–3] (e.g.,  $\text{La}_{2-x}\text{Sr}_x\text{CuO}_4$ ) and electron-doped [6–10] (e.g.,  $\text{Nd}_{2-x}\text{Ce}_x\text{CuO}_4$ ) share a similar temperature-doping phase diagram, which indicates a common origin of the superconducting pairing. However, the symmetry between hole- and electron-doped cuprates is only approximate. For example, superconductivity in electron-doped cuprates is much harder to achieve, since the antiferromagnetic phase persists at higher doping levels [8, 9, 11–13].

Perhaps the most puzzling anomaly of electron-doped cuprates is the fact that doping alone does not produce superconductivity [8, 9, 14]. As-grown samples are antiferromagnetic Mott insulators, and become superconducting only after high-temperature oxygen-reducing annealing [6, 7]. Annealing reduces the oxygen content by a small fraction [15–20] (between 0.1% and 2%), which contributes to additional electrons in the  $\text{CuO}_2$  layers [11, 12, 21–25], and to a de-

crease of the interlayer distance [26–31]. This results in a dramatic change of the electronic properties [32–38], including the emergence of the superconducting transition and a reduction of the Néel temperature [11, 39, 40], which cannot be achieved only by doping (e.g., by addition of extra cerium in  $\text{Nd}_{2-x}\text{Ce}_x\text{CuO}_4$  [29]). Furthermore, single crystals of the undoped parent compound  $\text{Nd}_2\text{CuO}_4$  are never superconducting. Conversely,  $\text{Nd}_2\text{CuO}_4$  thin films exhibit superconductivity after annealing, even without doping [14, 29]. In all cases, the annealing process must be carried in rather specific conditions that drive the samples almost to the limit of decomposition [41, 42]. For these reasons, it is clear that the annealing process must have additional effects. These may be the consequence of a reorganization of the crystal structure and/or a change of the distribution of dislocations and defects in the sample, such as the removal of the interstitial apical oxygens (defects) [17, 43–45], the removal of intrinsic in-plane oxygens [46–48], or the migration of copper ions to repair and reduce copper vacancies [49, 50]. A measurable effect of annealing is the change of the  $c$ -axis lattice parameter, which is 2 times the interlayer distance between  $\text{CuO}_2$  planes: The lattice parameter decreases to an optimal value  $c_{SC}$  at which superconductivity appears [14, 51]. Generally, oxygen reduction produces a decrease of the  $c$ -axis lattice parameter associated with the removal of apical oxygen [17, 18]: Hence, the value of  $c$  has been considered as a qualitative measure of the oxygen content [28, 30, 31].

In this work, we report the occurrence of superconductivity in oxygen-deficient  $\text{Nd}_{2-x}\text{Ce}_x\text{CuO}_4$  (NCCO) thin films, ob-

tained by annealing in oxygen-free atmosphere, and we provide a theoretical framework to describe the electronic properties and the structural changes before and after annealing. Our samples are grown by DC sputter deposition in oxygen-free atmosphere, and exhibit a  $c$ -axis lattice parameter shorter than the optimal value  $c_{SC}$ , which indicates oxygen deficiency, and the presence of a negligible amount of apical oxygens. Remarkably, these samples become superconducting after annealing in pure argon atmosphere, with a simultaneous *increase* of the  $c$ -axis parameter. This strongly indicates that the superconducting phase transition cannot be ascribed to a change of the oxygen content, but to a microscopic reorganization of the crystal structure induced by annealing. Moreover, in order to obtain a complete phase diagram as a function of the  $c$ -axis lattice parameter, we have grown thin films also in oxygen/argon atmosphere. These samples exhibit a  $c$ -axis lattice parameter longer than the optimal value  $c_{SC}$  and, as expected, become superconducting after annealing, with a *decrease* of the  $c$ -axis, in agreement with previous studies [6–9]. In all samples, the superconductivity is established only after the  $c$ -axis parameter reaches the optimal value  $c_{SC} = 12.08 \text{ \AA}$ . As we show using first-principles density functional theory (DFT), the evolution of the  $c$ -axis parameter and the presence of holes can be explained in terms of a microscopic structural modification, i.e., with existing oxygen ions partially migrating to apical positions with respect to  $\text{CuO}_2$  planes. This induces a remodulation of the energy bands and the suppression of antiferromagnetic order, allowing the emergence of hole superconductivity, i.e., the pairing of hole carriers within the same electronic band [34, 37, 38].

The undoped NCCO parent compound  $\text{Nd}_2\text{CuO}_4$  crystallizes in a tetragonal  $T'$  crystal structure, containing  $\text{CuO}_2$  layers stacked along the  $c$  axis and sandwiched between the charge reservoir layers, as shown in Fig. 1(a). Moreover, it is well-known that the lattice structure of NCCO thin films and other electron-doped materials exhibit disorder, with the presence of oxygen vacancies at regular sites ( $\text{CuO}_2$  layers or charge reservoir layers) as well as excess oxygen at apical sites above and below  $\text{CuO}_2$  layers [8, 9, 14], as shown in Fig. 1(b). In particular, the presence of in-plane oxygen vacancies is correlated to an increase of electrons in the conduction band [11, 12, 21–23, 25], whereas the concentration of oxygen ions on apical sites is correlated with the elongation of the  $c$ -axis parameter [28, 30, 31].

In our experiment, we used optimized DC sputtering to grow well-oriented NCCO films without spurious phases and with a fixed cerium content  $x = 0.17 \pm 0.01$ . We obtained films with thickness in the range 50–100 nm, grown respectively in pure argon (type A samples) and mixed argon/oxygen atmosphere with ratio  $\text{O}_2/\text{Ar} > 1\%$  (type B samples), at a total pressure of 1.7 mbar and heater temperature of 850 °C (see also Ref. 52 and 53 and Supplemental Material [54]).

In order to analyze the effect on the crystal structure of the reducing thermal treatment inducing superconductivity, the in-plane and the out-of-plane lattice parameters  $a$ ,  $b$ , and  $c$  are measured before and after annealing by x-ray diffrac-

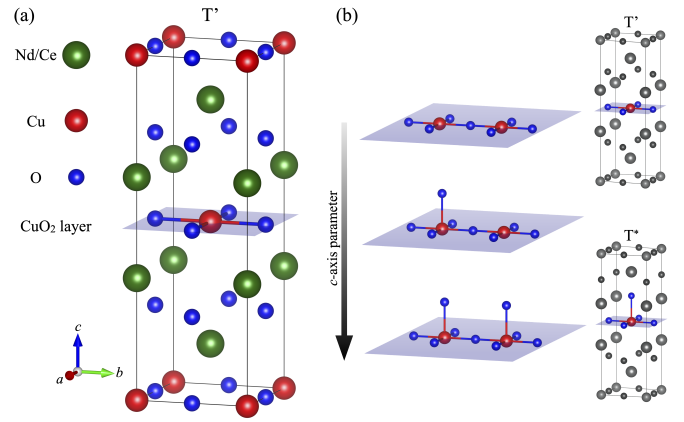


FIG. 1. (a) The NCCO parent compound (undoped  $\text{Nd}_2\text{CuO}_4$ ) crystallizes in the tetragonal  $T'$  structure.  $\text{CuO}_2$  layers are sandwiched between the charge reservoir  $\text{Nd}_{2-x}\text{Ce}_x\text{O}_2$  layers. Copper ions are surrounded by a square planar arrangement of oxygen ions in the  $ab$  plane. Oxygen ions are located within the  $\text{CuO}_2$  layers and the charge reservoir layers. (b) In doped compounds, oxygen ions may partially occupy apical sites above or below the Cu atoms, e.g., one apical oxygen for every two copper atoms, or every copper atom ( $T^*$  structure). The concentration of apical oxygens is correlated to the elongation of the  $c$ -axis parameter.

tion (XRD). We found for the as-grown type A samples  $c = 12.04\text{--}12.07 \text{ \AA}$  and  $a = b \approx 3.95\text{--}3.96 \text{ \AA}$ , while for the as-grown type B samples  $c = 12.09\text{--}12.15 \text{ \AA}$  and  $a = b \approx 3.94\text{--}3.97 \text{ \AA}$ . After annealing, type A samples grown in oxygen-free atmosphere exhibit a slight elongation of the  $c$ -axis, whereas the in-plane lattice parameter remains unchanged. Conversely, type B samples grown in oxygen atmosphere exhibit a systematic decrease of the  $c$ -axis after annealing, in agreement with previous results [26–31], and a small change of the in-plane lattice parameter in some of the samples. The analysis of  $(00l)$  reflections in XRD patterns [54] allows to obtain the  $c$ -axis lattice parameter of all superconducting films to be  $c_{SC} = 12.080\text{--}12.088 \text{ \AA}$ . As established by extensive studies on electron-doped films fabricated by molecular-beam epitaxy [55–57] and pulsed laser deposition [58–61], the  $c$ -axis lattice parameter can be used as a measure of the oxygen content. In these studies, the  $c$  parameter is always larger than the optimal superconducting value  $c_{SC}$ , as we also observe in type B over-oxygenated samples, and decreases with the concurrent elimination of excess oxygen atoms during annealing. Hence, a value  $c < c_{SC}$  in type A samples indicates oxygen-deficiency.

We measured the temperature dependence of the in-plane resistivity  $\rho(T)$  with a four-probe method in the temperature range 1.6–300 K, before and after annealing. As-grown nonsuperconducting type A samples (fabricated in oxygen-free atmosphere) exhibit a crossover between metallic and insulating regimes identified by a minimum of the resistivity  $\rho(T)$  at temperature  $T_{min}$ , and with a residual resistivity ratio  $RRR = \rho(300 \text{ K})/\rho(4.2 \text{ K}) > 1$ , as shown in Fig. 2(a). Furthermore, the resistivity exhibits a quadratic temperature dependence in the metallic region above  $T_{min}$ , as

it is clearly visible in Fig. 2(a). In electron-doped compounds, a quadratic resistivity dependence is usually found even above room temperature [8, 10, 62, 63]. As-grown nonsuperconducting type B samples (fabricated in mixed argon/oxygen atmosphere) exhibit instead a weak semiconductor-like temperature dependence on the resistivity with  $RRR < 1$  and  $\rho(T) \propto R(T) \propto T^{-\alpha}$ , as shown in Fig. 2(b).

The main effects of annealing are the modification of the oxygen content and the structural reorganization and redistribution of crystal defects and dislocations. In order to disentangle these two effects, we performed an ex-situ annealing in oxygen-free, pure argon flow. Despite different environmental growth conditions and different structural and electrical properties of type A and B samples, similar thermal treatments are needed to induce superconductivity. All samples become superconducting after annealing at high temperatures 900–950 °C, with 0.5–2 hours annealing time, depending on the film thickness. Moreover, all samples have similar critical temperatures  $T_c \lesssim 24$  K, as shown in Fig. 2(c). In contrast, no superconducting transition and no structural change are detected after annealing at temperatures below 900 °C and with the same environmental conditions, as reported elsewhere [64].

Figure 2(d-e) shows the phase diagram of our NCCO samples as a function of the  $c$ -axis lattice parameter, before and after annealing, which is the main experimental result of this work. In particular, Fig. 2(d) shows the residual resistivity ratio  $RRR$  as a function of the  $c$ -axis lattice parameter. In the region  $c < c_{SC}$  (sample type A), samples behave as weakly disordered metal with  $RRR \gtrsim 1$  and exhibit a metal-insulator crossover with minimum resistivity at  $T_{min}$ . We observe values of  $T_{min}$  up to 250 K and  $RRR \approx 1$ –2, with  $RRR$  increasing with decreasing  $T_{min}$ . In the region  $c > c_{SC}$  (sample type B), samples behave as disordered systems with  $RRR \lesssim 1$ , with a weakly semiconductor-like temperature dependence on the resistivity. Most importantly, Fig. 2(e) shows the superconducting critical temperatures  $T_c$  as a function of the  $c$ -axis lattice parameter. All samples achieve superconductivity after high-temperature annealing, accompanied by a structural change: An increase of  $c$ -axis for type A samples and a decrease for the type B samples. The superconducting regime is restricted to the value of lattice constant  $c_{SC} = 12.08$  Å. Hence, high-temperature annealing not only induces superconductivity, but also a concurrent and systematic increase (in type A samples) or decrease (in type B samples) of the  $c$ -axis lattice parameter toward the optimal value  $c_{SC}$ . This strongly suggests that the superconducting phase transition is induced by a structural reorganization and redistribution of oxygen atoms within the  $\text{CuO}_2$  layers, charge reservoir layers, and in the apical positions. Moreover, the correlation between the concentration of apical oxygens and the  $c$ -axis parameter clearly points to the crucial role and impact of apical oxygens on the electronic properties of the compound after annealing.

In order to understand the role of the structural reorganization of oxygen atoms, and in particular the effects of the presence/absence of apical oxygens on the properties of the three

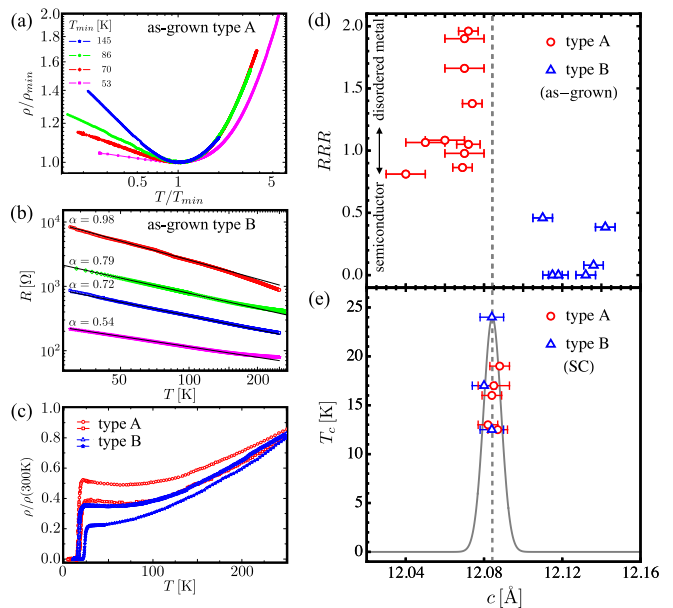


FIG. 2. (a) Resistivity as a function of temperature for type A samples, plotted on a log-log scale and normalized to the value of the minimum of the resistivity. (b) Resistance as a function of temperature for type B samples, plotted on a log-log scale. Continuous lines  $R(T) \propto T^{-\alpha}$  are the best fit to the data with slopes  $\alpha = 0.54, 0.72, 0.79, 0.98$ . (c) Normalized resistivity as a function of temperature for type A and B samples after annealing, showing the superconducting transition at  $T_c \lesssim 24$  K. (d) Residual resistivity ratio  $RRR$  for as-grown samples (both types) and (e) superconducting critical temperature  $T_c$  of samples after annealing, as a function of the  $c$ -axis lattice parameter. The dashed gray line corresponds to the average value of  $c_{SC}$  and the continuous smooth curve is a guide for the eye.

types of samples, we have theoretically modeled and studied the system by DFT using the VASP [65] package with plane-wave basis set and projector augmented wave method [66]. In particular, as-grown type A samples have been modeled by a  $T'$  structure as in Fig. 1, i.e., a crystal structure with no apical oxygens, according to its fabrication in oxygen-deficient atmosphere. Then, as-grown type B samples have been instead modeled by a  $T^*$  structure, i.e., a crystal structure with one apical oxygen for every copper atom, according to its fabrication in oxygen-rich atmosphere. Finally, superconducting samples have been modeled by a mixed  $T_{SC} = 2T^* + T'$  structure, with two  $T^*$  cells and one  $T'$  cell alternating along the  $c$ -axis, i.e., a crystal structure with two apical oxygens for every three copper atoms. This is justified by the experimental evidence that the  $c$ -axis lattice parameter and, consequently, the number of apical oxygens, assume intermediate values between those measured for type A and B samples. DFT calculations have been performed by first relaxing the crystal structure in order to obtain the lattice parameters and compare them with the actual ones and, in particular, with their characteristic hierarchical order. We also computed the antiferromagnetic moments  $m$  in order to monitor the intensity of the antiferromagnetic correlations, that could prevent

the emergence of superconductivity. The study of the  $T'$  and  $T^*$  phases of the undoped  $\text{Nd}_2\text{CuO}_4$  is reported in the Supplemental Material [54]. The  $T^*$  phase shows a larger band gap compared with the  $T'$  phase. The more correlated behavior of the  $T^*$  is confirmed by the magnetic moments, which are  $m = 0.38\mu_B$  and  $m = 0.43\mu_B$  for the  $T'$  and  $T^*$  phases respectively. Regarding the doped phase, Fig. 3(a) and (b) show the results for the  $T^*$  structure for  $x = 0.125$  and  $x = 0.25$ , respectively. In both cases, and reasonably for all intermediate doping (including  $x = 0.17$ ), we have (i) a quite large indirect band gap  $\Delta E_{XM}$  between the maximum of the lower Hubbard band at the point X (hole pocket) and the minimum of the upper Hubbard band at the point M (electron pocket), (ii) strong antiferromagnetic correlations ( $m = 0.34\mu_B$  and  $0.24\mu_B$ , respectively, for  $x = 0.125$  and  $0.25$ ), and (iii) hole pockets away from the Fermi level. This strongly correlated scenario accounts for the insulating behavior of as-grown type B samples. Figure 3(c) shows the results for the  $T'$  structure for  $x = 1/6 \approx 0.17$ . The gap  $\Delta E_{XM}$  has practically disappeared, although the antiferromagnetic correlations are still quite large ( $m = 0.27\mu_B$ ). However, hole pockets are still far from the Fermi level. Such a scenario accounts for the (poor) metallic behavior of as-grown type A samples. Finally, Fig. 3(d) shows the results for the  $T_{SC}$  structure for  $x = 1/6$ . The gap  $\Delta E_{XM}$  has completely disappeared, as well as the antiferromagnetic correlations for the  $T'$  region ( $m = 0.04\mu_B$ ), and hole pockets are available right at the Fermi level (at the symmetry point X). However, antiferromagnetic correlations in the  $T^*$  portion of the material are still relevant, being  $m = 0.36\mu_B$ . The presence of holes at the Fermi level and the suppression of antiferromagnetic correlations are fully compatible and can explain the emergence of hole superconductivity [34, 37, 38] in all samples after annealing. Moreover, confirming the validity and accuracy of the chosen modelization and the consistency of the obtained results, the *relaxed* values of the  $a$  and  $c$ -axis lattice parameters for  $x = 1/6$  are close to the experimental ones and, more importantly, in the same hierarchical order: For the  $T'$  structure (as-grown type A samples)  $a = b = 3.91 \text{ \AA}$  and  $c = 12.01 \text{ \AA}$ , for the  $T^*$  structure (as-grown type B samples)  $a = b = 3.83 \text{ \AA}$  and  $c = 12.26 \text{ \AA}$ , and for the  $T_{SC}$  structure (superconducting samples)  $a = 3.85 \text{ \AA}$  and  $c = 12.18 \text{ \AA}$ . The variation of the  $c$ -axis lattice parameter can be understood in terms of *level repulsion* between the bands with dominant  $T'$  character and those with dominant  $T^*$  character [see Fig. 3(d)] that leads to a remodulation of the overall band structure, which definitely weakens the antiferromagnetic correlations of the  $T'$  region and allows the emergence of holes right at the Fermi level (more details in the Supplemental Material [54]).

Concluding, the structural and the transport properties of NCCO samples shed new light on the microscopic mechanism underlying the annealing process, which is responsible for the onset of the superconductivity. Indeed, our experiments indicate that the removal of the excess oxygen is not sufficient to trigger superconductivity: Our oxygen-deficient samples, grown in oxygen-free atmosphere, become superconducting

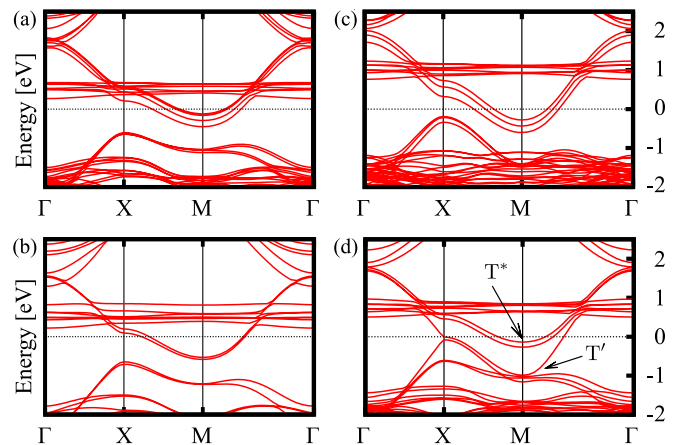


FIG. 3. DFT electronic band structure of NCCO for: (a)  $T^*$  structure with  $x = 0.125$ , (b)  $T^*$  structure with  $x = 0.25$ , (c)  $T'$  structure with  $x = 1/6 \approx 0.17$ , and (d)  $T_{SC} = 2T^* + T'$  structure with  $x = 1/6$ , where we highlighted the dominant  $T'$  and  $T^*$  bands with larger contributions. The Fermi level is set to zero. The flat bands at 0.5–1.5 eV above the Fermi level are the cerium  $4f$  bands. All other lower-energy bands are copper  $3d$  bands.

only after high-temperature annealing, which always occurs together with a change of the  $c$ -axis lattice parameter. This strongly indicates that the superconducting phase transition is induced by a microscopic structural reorganization, even in almost-optimally doped samples. This conclusion is supported by our theoretical analysis. Indeed, our DFT calculations show that the presence of a sizable number of apical oxygens is necessary to allow the emergence of hole superconductivity. In particular, no apical oxygens ( $T'$  structure), or too many of them ( $T^*$  structure), stabilize strong antiferromagnetic correlations and keep hole states away from the Fermi level, whereas an intermediate number of apical oxygens ( $T_{SC}$  structure) induces a suppression of antiferromagnetic correlations and allows to have holes available right at the Fermi level. This points to the relevance of interlayer hoppings mediated by apical oxygens, analogously to the scenario evidenced in hole-doped cuprates [67, 68]. Our experimental investigation and theoretical analysis provide strong evidence that the superconducting phase transition in electron-doped NCCO superconductors cannot be explained only in terms of changes of the oxygen content, but it necessarily requires a structural reorganization of the oxygen atoms in apical positions, which deeply affects the electronic properties of the compound.

A. G., A. L., and G. G. performed the experiments. A. G., A. N., and P. M. performed the experimental data analysis. C. A. and A. A. performed the DFT calculations. P. M., A. N., C. A., and A. A. wrote the manuscript. A. A. supervised the theoretical part. A. N. supervised the experimental part and the overall project. All coauthors contributed to the scientific discussion and final version of the manuscript. We thank M. Wysocki for useful discussions. C. A. is supported by the Foundation for Polish Science through the IRA Programme co-financed by EU within SG OP. C. A. acknowl-

edges the CINECA award under the IsC81 “DISTANCE” Grant for the availability of high-performance computing resources and support, and the support of the Interdisciplinary Centre for Mathematical and Computational Modeling (ICM), University of Warsaw, under Grants No. G73-23 and No. G75-10. P. M. is supported by the Japan Science and Technology Agency (JST) of the Ministry of Education, Culture, Sports, Science and Technology (MEXT), JST CREST Grant. No. JP-MJCR19T, by the (MEXT)-Supported Program for the Strategic Research Foundation at Private Universities Topological Science, Grant No. S1511006, and by JSPS Grant-in-Aid for Early-Career Scientists, Grant No. 20K14375. A. A. acknowledges support by MIUR under Project PRIN 2017RKWTMY.

\* These authors contributed equally to this work

† pmarra@ms-u.tokyo.ac.jp

‡ aavella@unisa.it

- [1] J. G. Bednorz and K. A. Müller, Possible high  $T_c$  superconductivity in the Ba–La–Cu–O system, *Z. Physik B* **64**, 189 (1986).
- [2] C. W. Chu, L. Z. Deng, and B. Lv, Hole-doped cuprate high temperature superconductors, *Physica C* **514**, 290 (2015).
- [3] A. Schilling, M. Cantoni, J. D. Guo, and H. R. Ott, Superconductivity above 130 K in the Hg–Ba–Ca–Cu–O system, *Nature* **363**, 56 (1993).
- [4] P. A. Lee, N. Nagaosa, and X.-G. Wen, Doping a Mott insulator: Physics of high-temperature superconductivity, *Rev. Mod. Phys.* **78**, 17 (2006).
- [5] T. Tohyama, Recent progress in physics of high-temperature superconductors, *Jpn. J. Appl. Phys* **51**, 010004 (2012).
- [6] H. Takagi, S. Uchida, and Y. Tokura, Superconductivity produced by electron doping in  $\text{CuO}_2$ -layered compounds, *Phys. Rev. Lett.* **62**, 1197 (1989).
- [7] Y. Tokura, A. Fujimori, H. Matsubara, H. Watabe, H. Takagi, S. Uchida, M. Sakai, H. Ikeda, S. Okuda, and S. Tanaka, Electron and hole doping in Nd-based cuprates with single-layer  $\text{CuO}_2$  sheets: Role of doped Ce ions and 30-K superconductivity, *Phys. Rev. B* **39**, 9704 (1989).
- [8] N. P. Armitage, P. Fournier, and R. L. Greene, Progress and perspectives on electron-doped cuprates, *Rev. Mod. Phys.* **82**, 2421 (2010).
- [9] P. Fournier, T’ and infinite-layer electron-doped cuprates, *Physica C* **514**, 314 (2015).
- [10] R. L. Greene, P. R. Mandal, N. R. Poniatowski, and T. Sarkar, The strange metal state of the electron-doped cuprates, *Annu. Rev. Condens. Matter Phys.* **11**, 213 (2020).
- [11] M. Horio, T. Adachi, Y. Mori, A. Takahashi, T. Yoshida, H. Suzuki, L. C. C. Ambolode, K. Okazaki, K. Ono, H. Kumigashira, H. Anzai, M. Arita, H. Namatame, M. Taniguchi, D. Ootsuki, K. Sawada, M. Takahashi, T. Mizokawa, Y. Koike, and A. Fujimori, Suppression of the antiferromagnetic pseudogap in the electron-doped high-temperature superconductor by protect annealing, *Nat. Commun.* **7**, 10567 (2016).
- [12] D. Song, G. Han, W. Kyung, J. Seo, S. Cho, B. S. Kim, M. Arita, K. Shimada, H. Namatame, M. Taniguchi, Y. Yoshida, H. Eisaki, S. R. Park, and C. Kim, Electron number-based phase diagram of  $\text{Pr}_{1-x}\text{LaCe}_x\text{CuO}_{4-\delta}$  and possible absence of disparity between electron- and hole-doped cuprate phase diagrams, *Phys. Rev. Lett.* **118**, 137001 (2017).
- [13] T. Helm, M. V. Kartsovnik, C. Proust, B. Vignolle, C. Putzke, E. Kampert, I. Sheikin, E.-S. Choi, J. S. Brooks, N. Bittner, W. Biberacher, A. Erb, J. Wosnitzer, and R. Gross, Correlation between Fermi surface transformations and superconductivity in the electron-doped high- $T_c$  superconductor  $\text{Nd}_{2-x}\text{Ce}_x\text{CuO}_4$ , *Phys. Rev. B* **92**, 094501 (2015).
- [14] M. Naito, Y. Krockenberger, A. Ikeda, and H. Yamamoto, Reassessment of the electronic state, magnetism, and superconductivity in high- $T_c$  cuprates with the  $\text{Nd}_2\text{CuO}_4$  structure, *Physica C* **523**, 28 (2016).
- [15] E. Moran, A. I. Nazzari, T. C. Huang, and J. B. Torrance, Extra oxygen in electron superconductors: Ce and Th doped  $\text{Nd}_2\text{CuO}_{4+\delta}$  and  $\text{Gd}_2\text{CuO}_{4+\delta}$ , *Physica C* **160**, 30 (1989).
- [16] J.-M. Tarascon, E. Wang, L. H. Greene, B. G. Bagley, G. W. Hull, S. M. D’Egidio, P. F. Miceli, Z. Z. Wang, T. W. Jing, J. Clayhold, D. Brawner, and N. P. Ong, Growth, structural, and physical properties of superconducting  $\text{Nd}_{2-x}\text{Ce}_x\text{CuO}_4$  crystals, *Phys. Rev. B* **40**, 4494 (1989).
- [17] P. G. Radaelli, J. D. Jorgensen, A. J. Schultz, J. L. Peng, and R. L. Greene, Evidence of apical oxygen in  $\text{Nd}_2\text{CuO}_y$  determined by single-crystal neutron diffraction, *Phys. Rev. B* **49**, 15322 (1994).
- [18] A. J. Schultz, J. D. Jorgensen, J. L. Peng, and R. L. Greene, Single-crystal neutron-diffraction structures of reduced and oxygenated  $\text{Nd}_{2-x}\text{Ce}_x\text{CuO}_y$ , *Phys. Rev. B* **53**, 5157 (1996).
- [19] P. W. Klamut, A. Sikora, Z. Bukowski, B. Dabrowski, and J. Klamut, On the properties of  $\text{Pr}_2\text{CuO}_{4\pm\delta}$  and  $\text{RE}_{2-x}\text{Pr}_x\text{CuO}_{4\pm\delta}$  synthesized under elevated oxygen pressure conditions, *Physica C* **282-287**, 541 (1997).
- [20] E. Navarro, D. Jaque, J. E. Villegas, J. I. Martín, A. Serquis, F. Prado, A. Caneiro, and J. L. Vicent, Oxygen content influence in the superconducting and electronic properties of  $\text{Nd}_{1.85}\text{Ce}_{0.15}\text{Cu}_{1.01}\text{O}_y$  ceramics, *J. Alloys Compd.* **323-324**, 580 (2001).
- [21] H. I. Wei, C. Adamo, E. A. Nowadnick, E. B. Lochocki, S. Chatterjee, J. P. Ruf, M. R. Beasley, D. G. Schlom, and K. M. Shen, Electron doping of the parent cuprate  $\text{La}_2\text{CuO}_4$  without cation substitution, *Phys. Rev. Lett.* **117**, 147002 (2016).
- [22] M. Horio, Y. Krockenberger, K. Koshiishi, S. Nakata, K. Hagiwara, M. Kobayashi, K. Horiba, H. Kumigashira, H. Irie, H. Yamamoto, and A. Fujimori, Angle-resolved photoemission spectroscopy of the low-energy electronic structure of superconducting  $\text{Pr}_2\text{CuO}_4$  driven by oxygen nonstoichiometry, *Phys. Rev. B* **98**, 020505(R) (2018).
- [23] M. Horio, Y. Krockenberger, K. Yamamoto, Y. Yokoyama, K. Takubo, Y. Hirata, S. Sakamoto, K. Koshiishi, A. Yasui, E. Ikenaga, S. Shin, H. Yamamoto, H. Wadati, and A. Fujimori, Electronic structure of Ce-doped and -undoped  $\text{Nd}_2\text{CuO}_4$  superconducting thin films studied by hard x-ray photoemission and soft x-ray absorption spectroscopy, *Phys. Rev. Lett.* **120**, 257001 (2018).
- [24] C. Lin, T. Adachi, M. Horio, T. Ohgi, M. A. Baqiya, T. Kawamura, H. Sato, T. Sumura, K. Koshiishi, S. Nakata, G. Shibata, K. Hagiwara, M. Suzuki, K. Ono, K. Horiba, H. Kumigashira, S. Ideta, K. Tanaka, Y. Koike, and A. Fujimori, Extended superconducting dome of electron-doped cuprates after protect annealing revealed by ARPES, arXiv:2006.04524 (2020).
- [25] K. Ishii, S. Asano, M. Ashida, M. Fujita, B. Yu, M. Greven, J. Okamoto, D.-J. Huang, and J. Mizuki, Post-growth annealing effects on charge and spin excitations in  $\text{Nd}_{2-x}\text{Ce}_x\text{CuO}_4$ , arXiv:2008.03420 (2020).
- [26] G. H. Kwei, S.-W. Cheong, Z. Fisk, F. H. Garzon, J. A. Goldstone, and J. D. Thompson, Structure and oxygen stoichiometry for the electron-doped cuprate superconductor  $\text{Nd}_{1.85}\text{Ce}_{0.15}\text{CuO}_{4-\delta}$ , *Phys. Rev. B* **40**, 9370(R) (1989).

- [27] E. Maiser, P. Fournier, J.-L. Peng, F. Araujo-Moreira, T. Venkatesan, R. Greene, and G. Czjzek, Pulsed-laser deposition of  $\text{Pr}_{2-x}\text{Ce}_x\text{CuO}_{4-y}$  thin films and the effect of high-temperature post-annealing, *Physica C* **297**, 15 (1998).
- [28] A. Tsukada, M. Noda, H. Yamamoto, and M. Naito, Role of impurity oxygen in superconductivity of “non-doped”  $\text{T}'$ - $(\text{La,RE})_2\text{CuO}_4$ , *Physica C* **426-431**, 459 (2005).
- [29] O. Matsumoto, A. Utsuki, A. Tsukada, H. Yamamoto, T. Manabe, and M. Naito, Synthesis and properties of superconducting  $\text{T}'$ - $\text{R}_2\text{CuO}_4$  ( $\text{R}=\text{Pr}$ ,  $\text{Nd}$ ,  $\text{Sm}$ ,  $\text{Eu}$ ,  $\text{Gd}$ ), *Phys. Rev. B* **79**, 100508(R) (2009).
- [30] O. Matsumoto, A. Utsuki, A. Tsukada, H. Yamamoto, T. Manabe, and M. Naito, Generic phase diagram of “electron-doped”  $\text{T}'$  cuprates, *Physica C* **469**, 924 (2009).
- [31] Y. Krockenberger, H. Irie, O. Matsumoto, K. Yamagami, M. Mitsuhashi, A. Tsukada, M. Naito, and H. Yamamoto, Emerging superconductivity hidden beneath charge-transfer insulators, *Scientific Reports* **3**, 2235 (2013).
- [32] J. Gauthier, S. Gagné, J. Renaud, M.-E. Gosselin, P. Fournier, and P. Richard, Different roles of cerium substitution and oxygen reduction in transport in  $\text{Pr}_{2-x}\text{Ce}_x\text{CuO}_4$  thin films, *Phys. Rev. B* **75**, 024424 (2007).
- [33] P. Richard, M. Neupane, Y.-M. Xu, P. Fournier, S. Li, P. Dai, Z. Wang, and H. Ding, Competition between antiferromagnetism and superconductivity in the electron-doped cuprates triggered by oxygen reduction, *Phys. Rev. Lett.* **99**, 157002 (2007).
- [34] Y. Dagan and R. L. Greene, Hole superconductivity in the electron-doped superconductor  $\text{Pr}_{2-x}\text{Ce}_x\text{CuO}_4$ , *Phys. Rev. B* **76**, 024506 (2007).
- [35] S. Charpentier, G. Roberge, S. Godin-Proulx, X. Béchamp-Laganière, K. D. Truong, P. Fournier, and P. Rauwel, Antiferromagnetic fluctuations and the Hall effect of electron-doped cuprates: Possibility of a quantum phase transition at underdoping, *Phys. Rev. B* **81**, 104509 (2010).
- [36] S. Asano, K. Ishii, D. Matsumura, T. Tsuji, T. Ina, K. M. Suzuki, and M. Fujita, Ce substitution and reduction annealing effects on electronic states in  $\text{Pr}_{2-x}\text{Ce}_x\text{CuO}_4$  studied by Cu K-edge x-ray absorption spectroscopy, *J. Phys. Soc. Jpn.* **87**, 094710 (2018).
- [37] Y. Li, W. Tabis, Y. Tang, G. Yu, J. Jaroszynski, N. Barišić, and M. Greven, Hole pocket-driven superconductivity and its universal features in the electron-doped cuprates, *Sci. Adv.* **5**, eaap7349 (2019).
- [38] J. Hirsch and F. Marsiglio, Understanding electron-doped cuprate superconductors as hole superconductors, *Physica C* **564**, 29 (2019).
- [39] M. Matsuda, Y. Endoh, K. Yamada, H. Kojima, I. Tanaka, R. J. Birgeneau, M. A. Kastner, and G. Shirane, Magnetic order, spin correlations, and superconductivity in single-crystal  $\text{Nd}_{1.85}\text{Ce}_{0.15}\text{CuO}_{4+\delta}$ , *Phys. Rev. B* **45**, 12548 (1992).
- [40] P. K. Mang, O. P. Vajk, A. Arvanitaki, J. W. Lynn, and M. Greven, Spin correlations and magnetic order in nonsuperconducting  $\text{Nd}_{2-x}\text{Ce}_x\text{CuO}_{4\pm\delta}$ , *Phys. Rev. Lett.* **93**, 027002 (2004).
- [41] J. S. Kim and D. R. Gaskell, The phase stability diagrams for the systems  $\text{Nd}_2\text{CuO}_{4-\delta}$  and  $\text{Nd}_{1.85}\text{Ce}_{0.15}\text{CuO}_{4-\delta}$ , *Physica C* **209**, 381 (1993).
- [42] P. K. Mang, S. Larochele, A. Mehta, O. P. Vajk, A. S. Erickson, L. Lu, W. J. L. Buyers, A. F. Marshall, K. Prokes, and M. Greven, Phase decomposition and chemical inhomogeneity in  $\text{Nd}_{2-x}\text{Ce}_x\text{CuO}_{4\pm\delta}$ , *Phys. Rev. B* **70**, 094507 (2004).
- [43] X. Q. Xu, S. N. Mao, W. Jiang, J. L. Peng, and R. L. Greene, Oxygen dependence of the transport properties of  $\text{Nd}_{1.78}\text{Ce}_{0.22}\text{CuO}_{4\pm\delta}$ , *Phys. Rev. B* **53**, 871 (1996).
- [44] J. B. Torrance and R. M. Metzger, Role of the Madelung energy in hole conductivity in copper oxides: Difference between semiconductors and high- $T_c$  superconductors, *Phys. Rev. Lett.* **63**, 1515 (1989).
- [45] Y. Ohta, T. Tohyama, and S. Maekawa, Apex oxygen and critical temperature in copper oxide superconductors: Universal correlation with the stability of local singlets, *Phys. Rev. B* **43**, 2968 (1991).
- [46] G. Riou, S. Jandl, M. Poirier, V. Nekvasil, M. Diviš, P. Fournier, R. Greene, D. Zhigunov, and S. Barilo, Infrared transmission study of  $\text{Pr}_2\text{CuO}_4$  crystal-field excitations, *Eur. Phys. J. B* **23**, 179 (2001).
- [47] G. Riou, P. Richard, S. Jandl, M. Poirier, P. Fournier, V. Nekvasil, S. N. Barilo, and L. A. Kurnevich,  $\text{Pr}^{3+}$  crystal-field excitation study of apical oxygen and reduction processes in  $\text{Pr}_{2-x}\text{Ce}_x\text{CuO}_{4\pm\delta}$ , *Phys. Rev. B* **69**, 024511 (2004).
- [48] P. Richard, G. Riou, I. Hetel, S. Jandl, M. Poirier, and P. Fournier, Role of oxygen nonstoichiometry and the reduction process on the local structure of  $\text{Nd}_{2-x}\text{Ce}_x\text{CuO}_{4\pm\delta}$ , *Phys. Rev. B* **70**, 064513 (2004).
- [49] K. Kurahashi, H. Matsushita, M. Fujita, and K. Yamada, Heat treatment effects on the superconductivity and crystal structure of  $\text{Nd}_{1.85}\text{Ce}_{0.15}\text{CuO}_4$  studied using a single crystal, *J. Phys. Soc. Jpn.* **71**, 910 (2002).
- [50] H. J. Kang, P. Dai, B. J. Campbell, P. J. Chupas, S. Rosenkranz, P. L. Lee, Q. Huang, S. Li, S. Komiya, and Y. Ando, Microscopic annealing process and its impact on superconductivity in  $\text{T}'$ -structure electron-doped copper oxides, *Nat. Mater.* **6**, 224 (2007).
- [51] Y. Krockenberger, M. Horio, H. Irie, A. Fujimori, and H. Yamamoto, As-grown superconducting  $\text{Pr}_2\text{CuO}_4$  under thermodynamic constraints, *Appl. Phys. Express* **8**, 053101 (2015).
- [52] A. Guarino, G. Patimo, A. Vecchione, T. Di Luccio, and A. Nigro, Fabrication of superconducting  $\text{Nd}_{2-x}\text{Ce}_x\text{CuO}_{4\pm\delta}$  films by automated dc sputtering technique, *Physica C* **495**, 146 (2013).
- [53] A. Guarino, A. Leo, G. Grimaldi, N. Martucciello, C. Dean, M. N. Kunchur, S. Pace, and A. Nigro, Pinning mechanism in electron-doped HTS  $\text{Nd}_{1.85}\text{Ce}_{0.15}\text{CuO}_{4-\delta}$  epitaxial films, *Supercond. Sci. Technol.* **27**, 124011 (2014).
- [54] See Supplemental Material below for more information.
- [55] M. Naito, H. Sato, and H. Yamamoto, MBE growth of  $(\text{La,Sr})_2\text{CuO}_4$  and  $(\text{Nd,Ce})_2\text{CuO}_4$  thin films, *Physica C* **293**, 36 (1997).
- [56] M. Naito, S. Karimoto, and A. Tsukada, Epitaxy-stabilized-n-type superconducting cuprates, *Supercond. Sci. Technol.* **15**, 1663 (2002).
- [57] Y. Krockenberger, H. Yamamoto, M. Mitsuhashi, and M. Naito, Universal superconducting ground state in  $\text{Nd}_{1.85}\text{Ce}_{0.15}\text{CuO}_4$  and  $\text{Nd}_2\text{CuO}_4$ , *Jpn. J. Appl. Phys.* **51**, 010106 (2011).
- [58] A. Gupta, G. Koren, C. C. Tsuei, A. Segmüller, and T. R. McGuire, Deposition of epitaxial thin films of  $\text{Nd}_{1.85}\text{Ce}_{0.15}\text{CuO}_{4-y}$  by laser ablation, *Appl. Phys. Lett.* **55**, 1795 (1989).
- [59] S. N. Mao, X. X. Xi, S. Bhattacharya, Q. Li, T. Venkatesan, J. L. Peng, R. L. Greene, J. Mao, D. H. Wu, and S. M. Anlage, Deposition and reduction of  $\text{Nd}_{1.85}\text{Ce}_{0.15}\text{CuO}_{4-y}$  superconducting thin films, *Appl. Phys. Lett.* **61**, 2356 (1992).
- [60] G. Roberge, S. Charpentier, S. Godin-Proulx, P. Rauwel, K. Truong, and P. Fournier, Improving the growth of electron-doped  $\text{Pr}_{2-x}\text{Ce}_x\text{CuO}_{4\pm\delta}$  thin films made by pulsed-laser deposition using excess  $\text{CuO}$ , *J. Cryst. Growth* **311**, 1340 (2009).
- [61] M. Hoek, F. Coneri, D. P. Leusink, P. D. Eerkes, X. R. Wang, and H. Hilgenkamp, Effect of high oxygen pressure anneal-

- ing on superconducting  $\text{Nd}_{1.85}\text{Ce}_{0.15}\text{CuO}_4$  thin films by pulsed laser deposition from Cu-enriched targets, *Supercond. Sci. Technol.* **27**, 044017 (2014).
- [62] P. L. Bach, S. R. Saha, K. Kirshenbaum, J. Paglione, and R. L. Greene, High-temperature resistivity in the iron pnictides and the electron-doped cuprates, *Phys. Rev. B* **83**, 212506 (2011).
- [63] T. Sarkar, R. L. Greene, and S. Das Sarma, Anomalous normal-state resistivity in superconducting  $\text{La}_{2-x}\text{Ce}_x\text{CuO}_4$ : Fermi liquid or strange metal?, *Phys. Rev. B* **98**, 224503 (2018).
- [64] A. Guarino, R. Fittipaldi, A. Romano, A. Vecchione, and A. Nigro, Correlation between structural and transport properties in epitaxial films of  $\text{Nd}_{2-x}\text{Ce}_x\text{CuO}_{4\pm\delta}$ , *Thin Solid Films* **524**, 282 (2012).
- [65] G. Kresse and J. Furthmüller, Efficiency of ab-initio total energy calculations for metals and semiconductors using a plane-wave basis set, *Comput. Mater. Sci.* **6**, 15 (1996).
- [66] G. Kresse and D. Joubert, From ultrasoft pseudopotentials to the projector augmented-wave method, *Phys. Rev. B* **59**, 1758 (1999).
- [67] E. Pavarini, I. Dasgupta, T. Saha-Dasgupta, O. Jepsen, and O. K. Andersen, Band-structure trend in hole-doped cuprates and correlation with  $T_{c\text{max}}$ , *Phys. Rev. Lett.* **87**, 047003 (2001).
- [68] S. Kim, X. Chen, W. Fitzhugh, and X. Li, Apical charge flux-modulated in-plane transport properties of cuprate superconductors, *Phys. Rev. Lett.* **121**, 157001 (2018).

# Superconductivity induced by structural reorganization in electron-doped cuprate NCCO: Supplemental Material

Anita Guarino<sup>1,2,\*</sup>, Carmine Autieri<sup>3,2,\*</sup>, Pasquale Marra<sup>4,5,†</sup>, Antonio Leo<sup>1,2,6</sup>, Gaia Grimaldi<sup>2,1</sup>, Adolfo Avella<sup>1,2,7,‡</sup> and Angela Nigro<sup>1,2</sup>

<sup>1</sup>*Dipartimento di Fisica “E. R. Caianiello”, Università degli Studi di Salerno, 84084 Fisciano (Salerno), Italy*

<sup>2</sup>*Consiglio Nazionale delle Ricerche CNR-SPIN, UOS Salerno, 84084 Fisciano (Salerno), Italy*

<sup>3</sup>*International Research Centre Magtop, Institute of Physics,*

*Polish Academy of Sciences, Aleja Lotników 32/46, 02668 Warsaw, Poland*

<sup>4</sup>*Graduate School of Mathematical Sciences, The University of Tokyo, 3-8-1 Komaba, Meguro, Tokyo, 153-8914, Japan*

<sup>5</sup>*Department of Physics, and Research and Education Center for Natural Sciences,*

*Keio University, 4-1-1 Hiyoshi, Yokohama, Kanagawa, 223-8521, Japan*

<sup>6</sup>*NANO\_MATES Research Center, Università degli Studi di Salerno, 84084 Fisciano (Salerno), Italy*

<sup>7</sup>*Unità CNISM di Salerno, Università degli Studi di Salerno, 84084 Fisciano (Salerno), Italy*

(Dated: December 25, 2020)

In this Supplemental Material, we include detailed information on the sample preparation, X-ray diffraction measurements, and computational details.

## SAMPLE PREPARATION

$\text{Nd}_{2-x}\text{Ce}_x\text{CuO}_4$  (NCCO) films with a fixed cerium content in the range 0.16–0.18 have been grown on (100)  $\text{SrTiO}_3$  substrates by DC sputtering technique. A single target of the stoichiometric  $\text{Nd}_{1.85}\text{Ce}_{0.15}\text{CuO}_4$  compound has been used as a sputtering source in an on-axis configuration with the substrate [1]. Films with thickness in the range 50–100 nm have been fabricated in pure argon (type A samples) or in mixed atmosphere of argon and oxygen ( $\text{O}_2$ ), with ratio  $\text{O}_2/\text{Ar} > 1\%$  (type B samples), both at a total pressure of 1.7 mbar and at a heater temperature of 850 °C. A first in-situ annealing is performed with a dwell time of 30 minutes at the same deposition temperature. In both cases, the superconductivity of the films was observed after a suitable ex-situ thermal treatments in flowing argon at a temperature above 900–950 °C. Despite different deposition conditions, the high annealing temperature is the same for all films, while an annealing time in the range 0.5–2 hours is used, depending on the film thickness.

Morphology, phase composition, and sample purity were inspected by scanning electron microscopy combined with wavelength-dispersive spectroscopy [1, 2], using an Oxford Scanning Electron Microscope Leo EVO 50 equipped with a wavelength-dispersive spectrometer. Structural properties are obtained by high-resolution X-ray diffraction technique in a Philips X’Pert-MRD diffractometer equipped with a four circle cradle.

The electrical transport properties were investigated in a Cryogenic Ltd. cryogen-free cryostat equipped with an integrated cryogen-free variable-temperature insert operating in the range 1.6–300 K. In this system, the sample is cooled by a continuous helium gas flow and the temperature stability is within 0.01 K. Sample temperature is measured via a LakeShore Temperature Controller model 350 connected to a LakeShore Cernox sensor. The electrical resistance measurements as a function of the temperature have been performed by a four-probe method, using a Keithley model 2430 as cur-

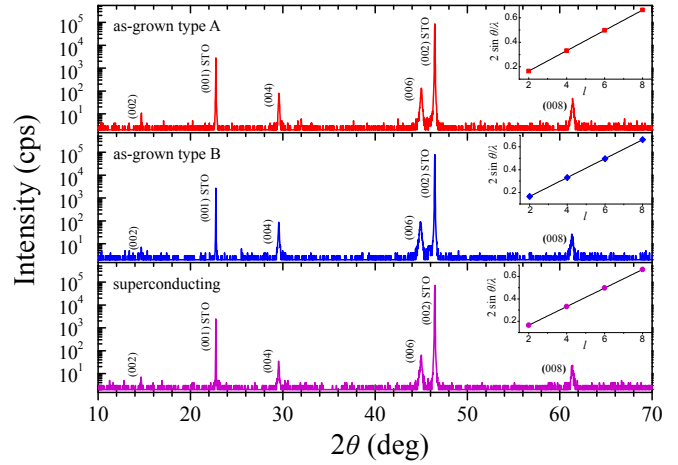


FIG. S1. X-ray diffraction patterns in units of counts per second for an as-grown type A sample, an as-grown type B sample, and a superconducting sample. The (001) and (002) peaks are due to the presence of the  $\text{SrTiO}_3$  substrate. Insets show the linear fit of  $2 \sin \theta / \lambda$  as a function of the Miller index  $l$ . The line slopes give the  $c$ -axis lattice parameter values.

rent source and a Keithley model 2182 as voltage meter. On selected films, in order to evaluate the resistivity, we realized microbridges with length  $L = 1$  mm, width  $W = 100 \mu\text{m}$  using a standard UV photolithography and wet etching in a 1% solution of  $\text{H}_3\text{PO}_4$  in pure water.

## X-RAY DIFFRACTION MEASUREMENTS

The structural properties of DC-sputtered NCCO films have been investigated by X-ray diffraction (XRD) technique. Figure S1 reports the typical  $\theta$ - $2\theta$  pattern of as-grown type A, as-grown type B, and superconducting samples. Besides the substrate reflections, XRD patterns of as-grown, nonsuperconducting samples show only the four (00 $l$ ) diffraction peaks with  $l = 2, 4, 6, 8$ , which are characteristic of the  $T'$  tetrago-

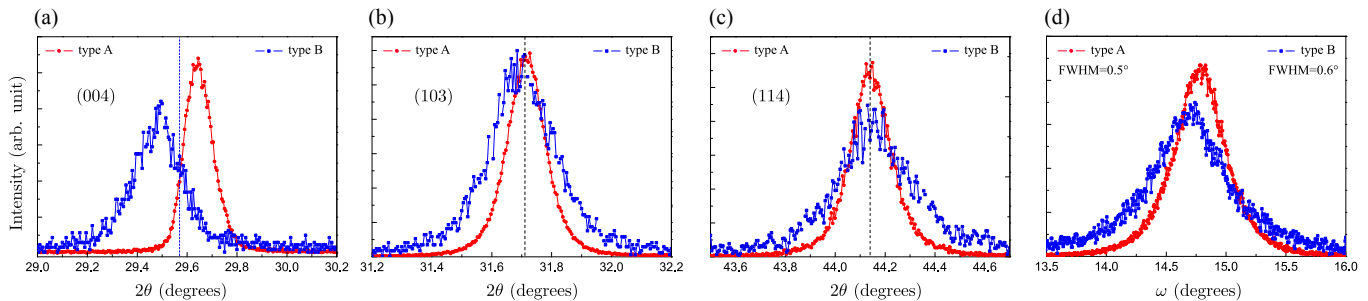


FIG. S2. Angular positions  $2\theta$  of the (004), (103), and (114) peaks in panels (a), (b) and (c) respectively, for a type A (red circles) and a type B sample (blue squares). Dashed lines correspond to the  $2\theta$  value measured in both samples after the annealing process. (d)  $\omega$ -scans around the (004) reflections for a type A (red circles) and a type B (blue squares) sample.

nal crystal structure, indicating a preferential growth with the  $c$ -axis perpendicular to the film surface and the absence of spurious phases.

The analysis of the  $(00l)$  reflections allows to obtain directly the  $c$ -axis lattice parameter from the Bragg law,  $2d\sin\theta = \lambda$ , with  $\lambda = 1.54056 \text{ \AA}$ ,  $\theta$  the half of the angular peak position  $2\theta$ , and with  $d = c/l$  in this case. Insets of Fig. S1 report the quantity  $2\sin\theta/\lambda$  as a function of the Miller index  $l$  together with the linear best fit of the data. The fitting parameter gives a different  $c$ -axis parameter for each sample. In particular, the  $c$ -axis parameter measured in the superconducting sample is  $c_{SC} = 12.079 \pm 0.005 \text{ \AA}$ . The value  $c = 12.069 \pm 0.005 \text{ \AA}$  obtained for the type A film is shorter than  $c_{SC}$ , while the  $c$ -axis parameter  $c = 12.09 \pm 0.01 \text{ \AA}$  of the type B sample is longer. Hence, the most oxygenated type B samples behave as typical samples reported in previous studies, where the measured as-grown  $c$ -axis parameter is longer than the value measured in superconducting samples [3–8]. A value  $c < c_{SC}$  is the peculiarity of our type A films.

Figure S2 shows the angular positions  $2\theta$  of the (004), (103), and (114) peaks respectively [(a) to (c)], for one type A and one type B as-grown samples compared with the value measured after annealing. We found for the as-grown type A sample  $c = 12.04 \pm 0.01 \text{ \AA}$  and  $a, b = 3.96 \pm 0.01 \text{ \AA}$ , while for the as-grown type B samples  $c = 12.11 \pm 0.01 \text{ \AA}$ ,  $a, b = 3.94 \pm 0.02 \text{ \AA}$ .

Figure S2(d) reports the measurement of the mosaicity of type A and B samples by the  $\omega$ -scan around the (004) reflection:  $\omega$  is the  $x$ -ray incident angle. Type A and B samples show a full width at half maximum (FWHM) equal to  $0.5^\circ$  and  $0.6^\circ$  respectively, indicating a more uniform  $c$ -axis orientation for type A samples (i.e., better epitaxial growth).

## COMPUTATIONAL DETAILS

We have performed first-principles density functional theory (DFT) calculations by using the VASP [9] package based on plane-wave basis set and projector augmented wave (PAW) method [10]. A plane-wave energy cut-off of 450 eV has been used for the atomic relaxation and 530 eV for the other cal-

culations. A  $k$ -point grid of  $8 \times 8 \times 2$  has been used for the atomic relaxation and  $10 \times 10 \times 4$  for the other calculations. For the treatment of exchange-correlation, Perdew-Burke-Ernzerhof [11] generalized gradient approximation for solid has been considered, since it is accurate for the structural relaxation of the  $A_2BO_4$  oxides bulk [12].

The analysis of the structural phases of compounds with  $4f$ -electrons is a nontrivial problem in DFT due to the difficulties to catch the position of the energetic levels of the  $f$ -electrons [13]. Few works studied electron-doped cuprate superconductors using *ab initio* techniques. Considering  $4f$  electrons in the core level, Bansil and coworkers were able to obtain the correct insulating groundstate for the undoped cases [14–16]. We use the PAW with 3 frozen  $f$ -electrons for the Nd and without frozen  $f$ -electrons for the Ce. Using the PAW without frozen electrons for the Ce, the  $T'$  phase is always the ground state. Using the PAW with three frozen  $f$ -electrons for the Ce, we obtain the stabilization of the  $T^*$  phase, but this does not allow the  $Ce^{+4}$  configuration experimentally observed.

We included the effects of the Hubbard  $U$  on the Cu sites. We scanned the values of  $U_{Cu}$  from 1 to 4 eV for the undoped and used  $J_H = 0.15U$  for the Cu- $3d$  states, and we assumed the value of  $U_{Cu} = 3.2 \text{ eV}$  because for this value the undoped  $T'$  phase is a narrow gap semiconductor. The Coulomb repulsion was applied also on the rare earth Nd and Ce (4 eV) and O (6 eV) but it is much less relevant since these electrons are far from the Fermi level.

To account the G-type antiferromagnetism in  $Nd_2CuO_4$  we use a  $\sqrt{2} \times \sqrt{2} \times 2$  supercell with 4 formula units. To investigate the structural properties as a function of doping, an additional calculation was done in the overdoped regime at  $x = 0.25$ . Using Vegard's law, we estimated the lattice constants for  $x = 0.17$ , which correspond to almost-optimally doping (as in our samples). Once we understood the structural properties, we study the electronic and magnetic properties of the compound relative to a value of the doping close to the experimental one. In order to do so, we used a  $\sqrt{2} \times \sqrt{2} \times 3$  supercell with 6 formula units. One Ce atom in 6 formula units will give the concentration of  $x = 1/6 \approx 0.17$ . This supercell can host 3 cuprate layers. However, in order to reproduce the  $T^*$  phase we need an even number of layers. As a consequence, the

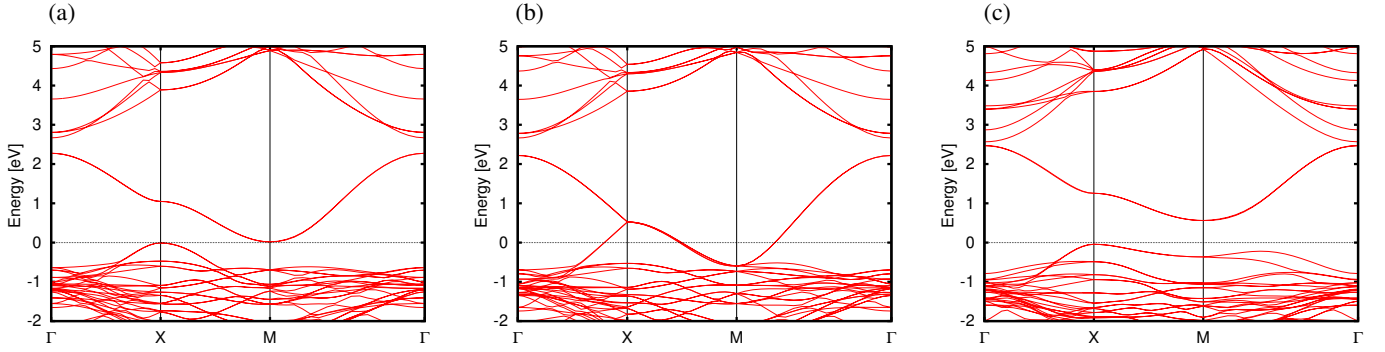


FIG. S3. (a) Band structure of the  $T'$  phase of the  $\text{Nd}_2\text{CuO}_4$  with antiferromagnetic order. The value of the Coulomb repulsion is  $U_{\text{Cu}} = 3.2 \text{ eV}$ . (b) Band structure of the  $T'$  phase of the  $\text{Nd}_2\text{CuO}_4$  with nonmagnetic atoms. The value of the Coulomb repulsion is  $U_{\text{Cu}} = 3.2 \text{ eV}$ . (c) Band structure of the  $T^*$  phase of the  $\text{Nd}_2\text{CuO}_4$  with antiferromagnetic order. The value of the Coulomb repulsion is  $U_{\text{Cu}} = 3.2 \text{ eV}$ .

$\sqrt{2} \times \sqrt{2} \times 3$  supercell cannot host the  $T^*$  phase but it can host the  $T'$  phase and a mixed phase with two  $T^*$  cells and one  $T'$  cell alternating along the  $c$ -axis. In this work, we call this phase the  $T_{SC} = 2T^* + T'$  phase.

The most stable configuration of the Ce atoms is obtained when the Ce atoms are far from each other. This means that during the growth the Ce atoms have a tendency to avoid each other, which points to a homogeneous distribution of these Ce atoms during the growth. In the most stable configuration of  $T^*$  phase, the Ce atoms are not in the apical oxygen layer. In the most stable configuration of the mixed  $T_{SC}$  phase, the Ce atoms are closer to the  $\text{CuO}_2$  layers of the  $T'$  phase.

#### DFT STUDY OF UNDOPED $\text{Nd}_2\text{CuO}_4$

In this Section, we present the results of the undoped  $\text{Nd}_2\text{CuO}_4$ . The  $T'$  and  $T^*$  phases of the  $\text{Nd}_2\text{CuO}_4$  have the same stoichiometry but a different atomic position of the oxygen atoms and consequently of the atomic layers. The  $T'$  phase consists of 4 atomic layers  $\text{CuO}_2/\text{O}/\text{Nd}_2/\text{O}$  while the  $T^*$  contains 3 atomic layers  $\text{CuO}_2/\text{NdO}/\text{NdO}$ . The different atomic composition of the atomic layers has a large influence on the lattice constant  $c$  and consequently on the in-plane lattice constant too. Considering just the effect of the packaging, we would expect that the  $T'$  phase with 4 atomic layers should have a larger  $c$  lattice constant, but we also need to consider the effect of the charge. In an oversimplified ionic picture, the  $\text{CuO}_2$  layers have a total charge  $-2$ , the O layers have charge  $-2$ , the  $\text{Nd}_2$  layers have charge  $+6$  while the  $\text{NdO}$  layers have charge  $+1$ . Therefore, the 4 layers of the  $T'$  phase have charge  $-2/-2/+6/-2$  while the 3 layers of the  $T^*$  phase have  $-2/+1/+1$ . Due to the greater charge, the 4 layers of the  $T'$  phase attract each other much more than the 3 layers of the  $T^*$  phase resulting in a shorter  $c$ -axis of the  $T'$  phase. Therefore, there is an interplay and competition between the charge and the volume effect: As a result, the  $T'$  phase has a shorter  $c$ -axis than the  $T^*$  phase. As a consequence of the shorter  $c$ , the  $T'$  phase presents a larger value of the in-plane lattice constant  $a$ . This simplified picture was verified in our DFT results. We performed structural relaxation for the undoped

case for the  $T'$  and  $T^*$  phases. We obtained  $a = 3.91 \text{ \AA}$  and  $c = 12.12 \text{ \AA}$  for the  $T'$  phase: The total volume is  $92.7 \text{ \AA}^3$  per formula unit. We obtained  $a = 3.83 \text{ \AA}$  and  $c = 12.34 \text{ \AA}$  for the  $T^*$  phase: The total volume is  $90.3 \text{ \AA}^3$  per formula unit.

The Cu states in  $T^*$  are more ionic due to the larger number of nearest-neighbor oxygen atoms, indeed the Cu  $d$ -orbitals are more localized and therefore the  $T^*$  phase is more insulating. Instead, the  $T'$  phase is a semiconductor. Once we fixed the equilibrium atomic positions, we investigate the electronic properties scanning the value of  $U_{\text{Cu}}$ . We search for the critical value of  $U_{\text{Cu}}^{cr}$  such that the  $T'$  phase is insulating, we get the value  $U_{\text{Cu}}^{cr} = 3.2 \text{ eV}$  for the  $T'$  phase and we assume this value for all the following calculations. The band structure of the semiconducting  $T'$  phase is shown in Fig. S3(a). We have the completely unoccupied upper Hubbard band between 0 and  $+2.2 \text{ eV}$  above the Fermi level due to the  $x^2 - y^2$  orbital in the minority spin channel. The lower Hubbard band due to the  $x^2 - y^2$  orbital in the majority spin channel is completely occupied and entangled with other occupied Cu  $d$ -bands. The band structure shows an indirect band gap with the maximum of the valence band at the X point and the minimum of the conduction band at the M point. The gap in the DFT approach is opened by the interplay between  $U_{\text{Cu}}$  and the antiferromagnetic order: Indeed, the  $T'$  phase without magnetism shows a metallic phase with robust holes at the X point as shown in Fig. S3(b). In the nonmagnetic phase, we also have a nonsymmetrical symmetry that produces a double degenerate band along the MX direction and a semi-Dirac point in X. Performing the antiferromagnetic calculation for the  $T^*$  phase, we obtain the band structure shown in Fig. S3(c). The band structure of the  $T^*$  phase shows a larger band gap and flatter Cu  $d$ -bands, but for the rest, we have the same properties as in the  $T'$  phase.

At  $U_{\text{Cu}} = 3.2 \text{ eV}$ , the energy difference between the antiferromagnetic and nonmagnetic phase is  $22 \text{ meV}$  per formula unit for the  $T'$  phase and  $70 \text{ meV}$  per formula unit for the  $T^*$  phase. Therefore, the  $T^*$  phase has a larger gap and its antiferromagnetic ground state is more robust. Increasing the value of  $U$ , the antiferromagnetic phase will become more stable but the scenario described here does not change qualitatively.

---

\* These authors contributed equally to this work

† pmarra@ms-u.tokyo.ac.jp

‡ aavella@unisa.it

- [1] A. Guarino, G. Patimo, A. Vecchione, T. Di Luccio, and A. Nigro, Fabrication of superconducting  $\text{Nd}_{2-x}\text{Ce}_x\text{CuO}_{4\pm\delta}$  films by automated dc sputtering technique, *Physica C* **495**, 146 (2013).
- [2] A. Guarino, C. Cirillo, A. Leo, S. Santandrea, G. Grimaldi, A. Polcari, R. Fittipaldi, C. Attanasio, P. Romano, A. Romano, A. Vecchione, and A. Nigro, Transport properties of over-doped epitaxial  $\text{NdCeCuO}$  films, *J. Supercond. Nov. Magn.* **24**, 169 (2011).
- [3] G. H. Kwei, S.-W. Cheong, Z. Fisk, F. H. Garzon, J. A. Goldstone, and J. D. Thompson, Structure and oxygen stoichiometry for the electron-doped cuprate superconductor  $\text{Nd}_{1.85}\text{Ce}_{0.15}\text{CuO}_{4-\delta}$ , *Phys. Rev. B* **40**, 9370(R) (1989).
- [4] E. Maiser, P. Fournier, J.-L. Peng, F. Araujo-Moreira, T. Venkatesan, R. Greene, and G. Czjzek, Pulsed-laser deposition of  $\text{Pr}_{2-x}\text{Ce}_x\text{CuO}_{4-y}$  thin films and the effect of high-temperature post-annealing, *Physica C* **297**, 15 (1998).
- [5] A. Tsukada, M. Noda, H. Yamamoto, and M. Naito, Role of impurity oxygen in superconductivity of “non-doped”  $\text{T}'\text{-(La,RE)}_2\text{CuO}_4$ , *Physica C* **426-431**, 459 (2005).
- [6] O. Matsumoto, A. Utsuki, A. Tsukada, H. Yamamoto, T. Manabe, and M. Naito, Synthesis and properties of superconducting  $\text{T}'\text{-R}_2\text{CuO}_4$  ( $\text{R}=\text{Pr, Nd, Sm, Eu, Gd}$ ), *Phys. Rev. B* **79**, 100508(R) (2009).
- [7] O. Matsumoto, A. Utsuki, A. Tsukada, H. Yamamoto, T. Manabe, and M. Naito, Generic phase diagram of “electron-doped”  $\text{T}'$  cuprates, *Physica C* **469**, 924 (2009).
- [8] Y. Krockenberger, H. Irie, O. Matsumoto, K. Yamagami, M. Mitsuhashi, A. Tsukada, M. Naito, and H. Yamamoto, Emerging superconductivity hidden beneath charge-transfer insulators, *Scientific Reports* **3**, 2235 (2013).
- [9] G. Kresse and J. Furthmüller, Efficiency of ab-initio total energy calculations for metals and semiconductors using a plane-wave basis set, *Comput. Mater. Sci.* **6**, 15 (1996).
- [10] G. Kresse and D. Joubert, From ultrasoft pseudopotentials to the projector augmented-wave method, *Phys. Rev. B* **59**, 1758 (1999).
- [11] J. P. Perdew, A. Ruzsinszky, G. I. Csonka, O. A. Vydrov, G. E. Scuseria, L. A. Constantin, X. Zhou, and K. Burke, Restoring the density-gradient expansion for exchange in solids and surfaces, *Phys. Rev. Lett.* **100**, 136406 (2008).
- [12] C. Autieri, M. Cuoco, and C. Noce, Structural and electronic properties of  $\text{Sr}_2\text{RuO}_4/\text{Sr}_3\text{Ru}_2\text{O}_7$  heterostructures, *Phys. Rev. B* **89**, 075102 (2014).
- [13] K. P. Kramer, M. Horio, S. S. Tsirkin, Y. Sassa, K. Hauser, C. E. Matt, D. Sutter, A. Chikina, N. B. M. Schröter, J. A. Krieger, T. Schmitt, V. N. Strocov, N. C. Plumb, M. Shi, S. Pyon, T. Takayama, H. Takagi, T. Adachi, T. Ohgi, T. Kawamata, Y. Koike, T. Kondo, O. J. Lipscombe, S. M. Hayden, M. Ishikado, H. Eisaki, T. Neupert, and J. Chang, Band structure of overdoped cuprate superconductors: Density functional theory matching experiments, *Phys. Rev. B* **99**, 224509 (2019).
- [14] T. Das, R. Markiewicz, and A. Bansil, Intermediate coupling model of the cuprates, *Adv. Phys.* **63**, 151 (2014).
- [15] A. A. Kordyuk, Electronic band structure of optimal superconductors: From cuprates to ferropnictides and back again, *Low Temp. Phys.* **44**, 477 (2018).
- [16] J. W. Furness, Y. Zhang, C. Lane, I. G. Buda, B. Barbiellini, R. S. Markiewicz, A. Bansil, and J. Sun, An accurate first-principles treatment of doping-dependent electronic structure of high-temperature cuprate superconductors, *Commun. Phys.* **1**, 11 (2018).